



1 Muography as a new tool to study the historic earthquakes
2 recorded in ancient burial mounds

3

4 Hiroyuki K.M. Tanaka^{1,2}, Kenji Sumiya³, László Oláh^{1,2}

5

6 ¹Earthquake Research Institute, The University of Tokyo, 1-1-1 Yayoi, Bunkyo, Tokyo
7 113-0032, Japan

8 ²International Muography Research Organization (MUOGRAPHIX), The University of
9 Tokyo, 1-1-1 Yayoi, Bunkyo, Tokyo 113-0032, Japan

10 ³Graduate School of Informatics, Kansai University, 2-1-1 Ryozenji-cho, Takatsuki-shi,
11 Osaka 569-1095, Japan

12

13

14 **Abstract**

15 Bidirectional muographic measurements were conducted at the Imashirozuka burial
16 mound, Japan. The mound was built in the beginning of the 6th century as a megalithic
17 tomb and was later collapsed after a landslide caused by the 1596 Fushimi Earthquake,
18 one of the largest earthquakes that have occurred in Japan over last few centuries. The
19 measurements were conducted in order to find evidence of this past disaster recorded in
20 this historical heritage sites. As a result, the vertical low-density regions were found at
21 the top of the mound. These regions were interpreted as large-scale vertical cracks that
22 caused the translational collapse process behind the rotational landslide that was already
23 found in the prior trench-survey-based works. These results indicate that there was an
24 intrinsic problem with the stability of the basic foundation of the Imashirozuka mound
25 before the 1596 Fushimi Earthquake.

26

27

28 **1. Introduction**

29 By expanding our understanding of past large-scale natural disasters, such as tsunami,
30 earthquakes and volcanic eruptions, future hazards can be extrapolated and estimated.
31 However, modern scientific records of these natural disasters only, for the most part,
32 cover events from the last couple of centuries, which have been recorded by scientific
33 instruments only in limited regions throughout the world. However, geographical or



34 topographical modifications are often physically recorded in the land surface as a result
35 of such large-scale natural disasters, and correct methodologies can be deciphered to
36 infer unknown details about these events. For example, a large-scale volcanic eruption
37 usually creates a large volume pyroclastic flow, which later remains in the geological
38 stratum as a sedimentation of volcanic products. By applying a geological dating
39 technique to these past remnants of the eruptions, we can infer the timing and the
40 magnitude of the past disasters. However, the geological timescale is largely different
41 from that of human history, and the dating precision by these geochronological
42 techniques is limited to an order of 100 years. On the other hand, historical studies often
43 provide records that can be verified with yearly or sometimes, daily precision,
44 depending on how far back the disaster occurred. Historical information is more
45 straightforward regarding affected sites and the year or date of the disaster. For example,
46 this information can come from literature, which describes destruction by earthquakes
47 or repairs after earthquakes, providing valuable evidence for the location of earthquakes
48 and the effects brought by these earthquakes. Therefore, if we can combine the
49 historian's knowledge with the analysis results of these past disaster remnants, historical
50 records become valuable information which can help to improve the accuracy of these
51 geological dating techniques by developing into an iteration process. The derivation by
52 scientists and engineers have been utilized as evidence of earthquakes and which are
53 later incorporated by historian to evaluate the dates of the events, and vice versa.

54

55 Thus far, a combination of geological techniques and historical data have been applied
56 to historically well-studied objects to fill the gaps in our understanding of the historical
57 natural disaster record including tsunami (Daly et al., 2019; Dey et al. 2014),
58 earthquakes (Korjenkov and Mazor, 2003; Guidoboni et al., 1994; Ambraseys et al.
59 1983) and volcanic eruptions (Elson and Ort, 2018). The data are exploited mostly by
60 direct excavation of the historic site, and such anatomical techniques (similar in
61 principle to dissecting bodies to directly view organs within human bodies) allow us to
62 exploit regional, direct and detailed information; however, not all historical heritage
63 sites can be accessible and modified in this way. For example, due to the cultural
64 restriction, it is not always possible to conduct a trench survey to excavate the extant
65 historical structures such as the ancient monuments or public buildings to obtain the
66 geological knowledge about the past disaster remnants. Even when such a style of
67 investigation is approved, the exploitable information is usually localized. Thus, there is
68 a need for a non-invasive technique such as surface wave exploration, which would be
69 conducted to provide a more overall picture of targeted structures to increase the



70 possibilities of finding more physical evidence of past disasters.

71

72 Muography is a technique enabling us to "x-ray" gigantic (hectometric to kilometric)
73 objects. The surface of the Earth is constantly bombarded with muons, particles that
74 have decayed from cosmic rays arriving at the atmosphere from outside our solar
75 system, and these particles can be utilized as probes for muography. After traversing
76 targeted object, remnant muons are tracked with a particle detector located at lower
77 elevations than the region of interest inside the target. The result is a pattern of the
78 contrast in the density distribution inside the objects, which is projected on a
79 2-dimensional plane. Muography has been applied to image the internal structure of
80 volcanoes (Tanaka et al. 2007; Tanaka et al., 2009; Lesparre et al., 2012; Tanaka et al.,
81 2014; Olah et al., 2019), cultural heritages including Giza pyramids (Cheops and
82 Chephren), Egypt, Prambanan temples, Indonesia, Mt Echia, Italy and Santa Maria del
83 Fiore, Italy (Alvarez et al., 1970; Hanazato and Tanaka, 2016; Tanaka and Ohshiro,
84 2016; Morishima et al., 2017; Guardincerri et al. 2018; Cimmino et al. 2019), industrial
85 plants (Tanaka, 2013), and other natural (Tanaka et al., 2011; Olah et al. 2012; Schouten,
86 2018) and man-made structures (Mohon et al. 2018). Prior works have focused on
87 searching undiscovered chambers or the total weight of the heritage. Instead, in this
88 work, we applied muography to study ancient earthquakes for the first time. We focused
89 on the 1596 Fushimi Earthquake, one of the largest earthquakes that have occurred in
90 Japan over last few centuries and examine whether the technique of muography can
91 increase the possibilities of finding more physical evidence of past disasters recorded in
92 historical heritage sites.

93

94 **2. Observation**

95 Imashirozuka, an imperial burial mound in Japan was chosen as a target of the current
96 study. In Japan, imperial burial mounds have been well studied and a lot of knowledge
97 has accumulated. For the current study, this type of the burial mound has the following
98 advantages to study past earthquakes (Kamai et al., 2008). (A) The construction method
99 of the imperial mound is well studied by historians and thus, even if the mound has been
100 damaged by the past earthquakes, the original structure of the mound can be estimated.
101 (B) The imperial mound was built as a stable object, and thus collapsed areas inside the
102 mound would be likely to be records of past major earthquakes. (C) The imperial
103 mounds are in general situated in the urban area. Therefore, the collapsed mounds can
104 be used as an index to measure the past seismic disasters in urban areas long ago. (D) In
105 the recent human's history, various kinds of embankments have been built, but its



106 stability is discussed within the time scale of decades. The collapsed mounds offer us a
107 unique opportunity of geotechnical discussions within a time scale of centuries. (E) The
108 construction method of the mound was already well established when they were built.
109 The mounds built in the same era used the same construction method and thus it is
110 expected that the mechanical strength is the same. Therefore, the different collapsing
111 conditions among different mounds located near each other could infer different ground
112 conditions or different underwater conditions.

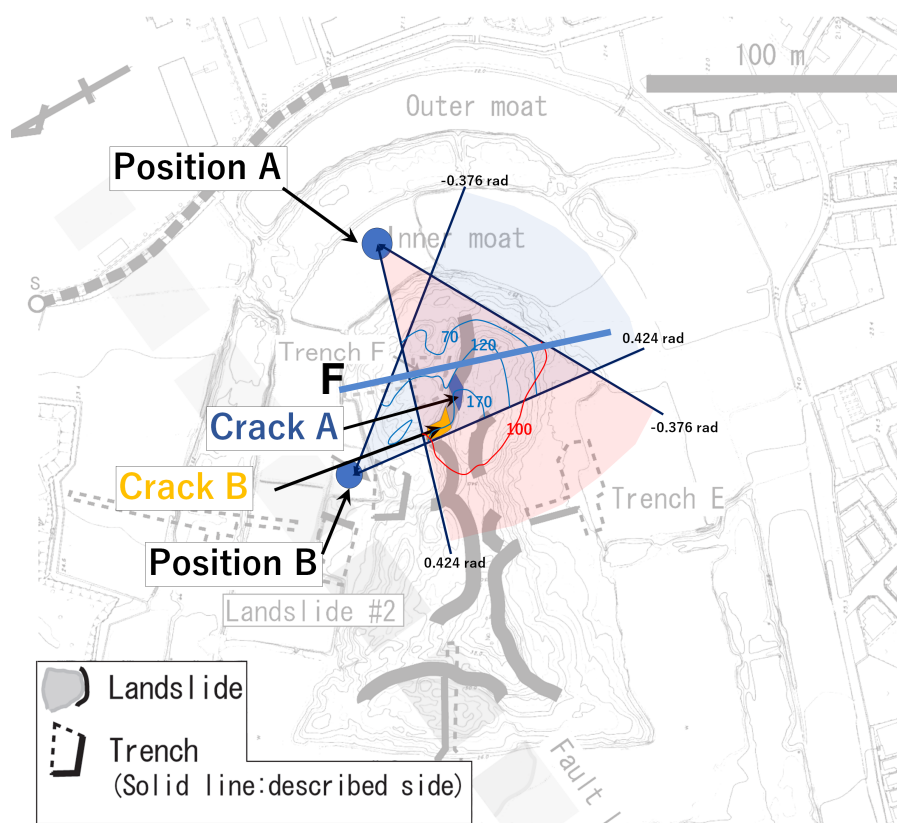
113

114 Imashirozuka is a keyhole-shaped imperial burial mound that was built in the beginning
115 of the 6th century in Japan. This burial mound is situated on one of the most active
116 faults in Japan, which is part of the Rokkou active fault system. This fault system
117 caused the Great Hanshin Earthquake in 1995. In 1596, it is thought that this Rokkou
118 active fault system and the next neighbor fault system called the Arima-Takatsuki
119 tectonic line were activated at the same time, and one of the largest earthquakes in the
120 last few centuries, Fushimi Earthquake, (Magnitude 7.25-7.75) occurred (Kamai et al.,
121 2008). The total length of the Imashirozuka mound is 190 m and the height is 11-12 m.
122 Although this burial mound was originally built in the triple-layered structure, the top
123 layer collapsed after a landslide. The collapse occurred more extensively in the northern
124 part of the mound. The level of damage depends, in general, on the ground motion
125 during an earthquake, which itself depends on its magnitude and distance from the site.
126 This extensive collapse is probably due to the existence of the Ai fault line, a part of the
127 Rokkou active fault system, is located closer to the northern part of the mound.
128 Currently, Imashirozuka mound consists of a base layer made of high bulk density
129 sandy clay (a soil particle density of 2.6 gcm^{-3} with a porosity of 52%), and a middle
130 layer made of lower bulk density granules (a soil particle density of $2.6\text{-}2.8 \text{ gcm}^{-3}$ with a
131 porosity of 76%) (Kamai et al., 2008). The s-velocity structure observed in the base
132 layer was faster (harder) in comparison to the middle layer (Kamai et al., 2008). For
133 the purpose of the archaeological studies, 6 trenches were excavated and landslide
134 remnants were observed in many of these trenches. The burial mound was originally
135 surrounded by a double moat, but most of this moat was buried in the past, and only a
136 part of it currently remains. The landslide deposits originated from the sediments in the
137 moat were dated, and the results were 1420-1510 AD with a method of the C^{14} dating
138 (Sangawa and Miyazaki 2001). Since it is known that Fushimi Earthquake occurred in
139 1596, this burial mound collapse was thought to have been triggered by this earthquake
140 (Sangawa and Miyazaki 2001).

141



142 The top view of the scalps and landslides generated by the 1596 Fushimi Earthquake is
143 shown in Figure 1 (Kamai et al., 2008). The results of the trench survey indicated that
144 most of the landslide types were represented by a combination of translational and
145 rotational landslides (Kamai et al., 2008). Movement was inferred with the following
146 sequence: 1. the landslide mass moved near horizontally for a few meters, 2. the
147 transported landslide mass reached the inner moat, 3. the landslide mass slid down and
148 shifted from translational to rotational landslide mode. Conversely, It was found that an
149 exceptionally large-scale rotational landslide occurred in the northern region of the
150 round-shaped section of the burial mound (Scalps A and B in Figure 1). Whether the
151 burial mound deformation related to this rotational slide is connected to the translational
152 landslide had continued to be a mystery. The purpose of this work was to examine
153 whether muographically found evidence can be used to address this question.
154



155
156 Figure 1. Top view of Imashirozuka burial mound. Positions A and B indicate the

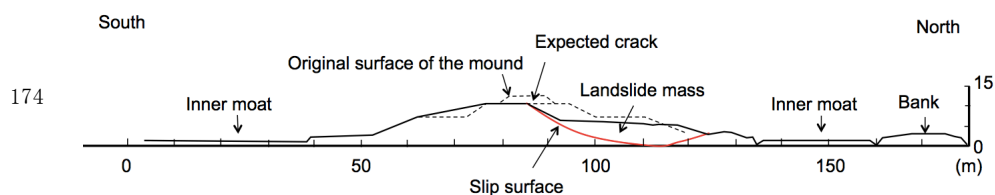


157 locations of the detectors for the current bidirectional muographic observations. The
158 shaded areas in red and blue indicate the viewing angle of each measurement. The solid
159 curves indicate the cross-sectional view of the mound at given elevation angles from
160 Positions A (red) and B (blue). The numbers indicate the elevation angles in units of
161 mrad.

162

163 In Figure 2, the cross-sectional view of the mound sliced along Line F in Figure 1 is
164 shown. This structure has been modeled based on the trench surveys conducted in 2008
165 (Kamai et al. 2008). Original surface of the mound (dashed lines in Figure 2) that was
166 estimated from the past archaeological studies, was lost by the landslide triggered by the
167 1596 Fushimi earthquake. The red lines indicate the slip surface of the landslide and at
168 the top of this surface, the existence of near-vertical cracks was expected. From these
169 trench surveys, the region indicated between the red lines and the solid black lines in
170 this figure was interpreted as the landslide mass, and displayed lower density than the
171 other part of the mound and thus, it was expected that muons could penetrate more in
172 this region (in particular at the top of this region).

173



174
175 Figure 2. Cross-sectional view of the mound along Line F in Figure 1. The dashed lines
176 indicate the original surface of the mound, and the red lines indicate the slip surface of
177 the landslide triggered by the 1596 Fushimi earthquake. The authors drew this image
178 based on the work done by Kamai et al. (2008).

179

180 Mechanical fractures within rock and soil produce a significant amount of interparticle
181 space and these fractured zones are detected as lower-density-regions in muographic
182 images (Tanaka and Muraoka, 2013, Carbone et al. 2014). Likewise, when a landslide
183 occurs, various processes influence changes in the density distribution inside a burial
184 mound. When a crack is generated in the burial mound, the density is reduced along the
185 crack. If a large-scale collapse occurs, the collapsed landslide mass will contain a lot of
186 inter-particle voids, and the density will be reduced. If the geometrical arrangement is
187 altered between the high-density base layer and lower density middle layer due to the
188 ground motion such as a fault slip, the overall density distribution will be altered



189 accordingly. All of these variations can be imaged with muography.

190

191 **3. Method**

192 Bidirectional muographic measurements were conducted at the Imashirozuka burial
193 mound site so that the resultant images could be used for 3-dimensional interpretation of
194 the internal structure of the circular section of the mound. In particular, one of the
195 detector positions of the current bidirectional measurements were chosen on the
196 northern side of the round-shaped section (Position B) so that the area where the
197 extensive collapse occurred could be more closely observed. The positions chosen for
198 the current measurement are shown in Figure 1. The first measurement of the
199 Imashirozuka mound started at Position A on September 21, 2019. The data were taken
200 for 40 days, and subsequently the detector was moved to Position B to collect the data
201 for another period of approximately one month.

202

203 The detector employed for the current measurement was the multi-wire proportional
204 chambers (MWPC) based muographic observation system (MMOS) that consists of 6
205 layers of MWPCs and lead plates with a total thickness of 10 cm. A detailed description
206 of the MMOS can be found in elsewhere (Olah et al. 2018), and thus only the main
207 features are briefly introduced here. In between each of the MWPC, a 2-cm thick lead
208 plate accommodated in a 4 mm-thick-stainless steel case is inserted, thus the total
209 thickness of these radiation shields is equivalent to $\sim 130 \text{ gcm}^{-2}$. These radiation
210 shields function as an absorber or a scatterer of low energy background particles that
211 include muons or other electromagnetic particles. Only the straight trajectories
212 throughout 6 detectors are employed and recorded as muons. In the current
213 measurements, the total weight of the MMOS was 600 kg including the case, batteries
214 and gas bottle. The total power consumption of the detector was $\sim 30\text{W}$, and the six
215 400-Wh lithium-ion batteries loaded into the case allowed us the continuous operation
216 for 80 hours, and the recurrent charging and replacements of the batteries further
217 extended the time of the continuous operation. The flow rate of the Ar-CO₂ gas mixture
218 (Ar:80, CO₂:20) through the chambers was 1–2 liters per hour to enable continuous
219 operation for a few months with a standard 40L type (6,000 liters) gas bottle. The
220 casters attached to the bottom of the case facilitated movements of the detector around
221 the mound. Moisture absorbent boxes were equipped inside the box in order to retain
222 the humidity at a constant level around the MWPCs. The size of the active area of the
223 detector was $80 \times 80 \text{ cm}^2$, and the distance between the uppermost and lowermost
224 stream detectors were 150 cm. The recorded muon tracks were stored and the numbers



225 of muon counts were directionally sorted out into a matrix with an angular binning
226 width of 8 x 8 mrad. As is indicated in Figure 1, the azimuthal viewing angle was
227 +/-500 mrad, however, due to the smaller geometrical acceptance for larger angles, only
228 the data within +/-400 mrad were used. The detector cost was ~60k US dollars, but the
229 operational cost was suppressed to a few thousand US dollars for entire operation
230 including the transportation, human resources for battery replacements and data
231 download.

232

233 Since the current target size is an order of 100 m, the following simplified analytical
234 expression can be applied for derivation of the relative density variations inside the
235 target volume because the muon's cutoff energy (the minimum energy of the muons that
236 can escape from the target volume) is much lower than the critical energy, 708 GeV in
237 SiO₂, the continuous ionization process is the main energy loss process (Tanaka and
238 Ohshiro, 2016).

239

$$240 \quad I_0/I_1=(X_0/X_1)^{-\gamma}, \quad (1)$$

241

242 where I_0 and I_1 is the remnant muon flux after passing through different densimetric
243 thickness of rock X_0 and X_1 . The Greek symbol, γ , is the zenith-angular dependent index
244 of the power law of the integrated muon spectrum within 50-200 GeV. In this work,
245 only the “relative muon flux” was used for discussions of the density contrast inside the
246 mound. The obtained matrix has been normalized by the azimuthal distribution of the
247 open-sky flux so that the azimuthally angle-dependent acceptance has been canceled in
248 the image.

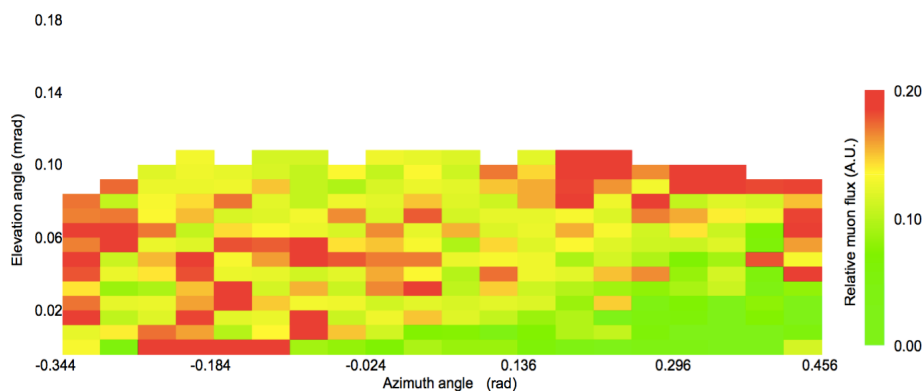
249

250 **4. Results**

251 Figure 3 shows the muographic image (Image A) taken at Position A that is indicated in
252 Figure 1. Corresponding azimuthal angles (-0.344 rad - 0.456 rad) are shown in Figure 1.
253 The distance between the detector and the peak of the mound was 70 m, and thus the
254 elevation angle of the mound peak was ~110 mrad (~6 degrees). Since the convex level
255 of the mound is small, the matrix was not re-binned in the elevational direction, but was
256 re-binned in 40 mrad in the azimuthal direction in order to increase the statistics. The
257 data were normalized to the azimuthal distribution of the open-sky muon tracks that was
258 unaffected by the existence of the mound, which corresponds to the elevational region
259 between 300 and 360 mrad in order to derive the “relative muon flux”. The bottom right



260 green-colored region in Figure 3, where the number of muons was counted less than
261 other regions corresponds to the direction, where the background mound (rectangular
262 section) was overlapped to the foreground mound (circular section); hence longer path
263 lengths for muons, as can be seen in Figure 1. The reddish patch that can be seen on the
264 left side of this green-colored region indicates a low-density collapsed landslide mass
265 on the northern slope of the mound. It was expected that the region around scarp
266 (arc-shaped lines in Figure 1) had cracks, and thus the average density along these
267 cracks was significantly lower than the density around these. This density reduction
268 effect is maximized in muographs when the muon's ray path is parallel to these cracks.
269 From Position A, this direction corresponds to the azimuthal angular range between 200
270 mrad and 300 mrad (see the position indicated by "Crack A" in Figure 1).
271



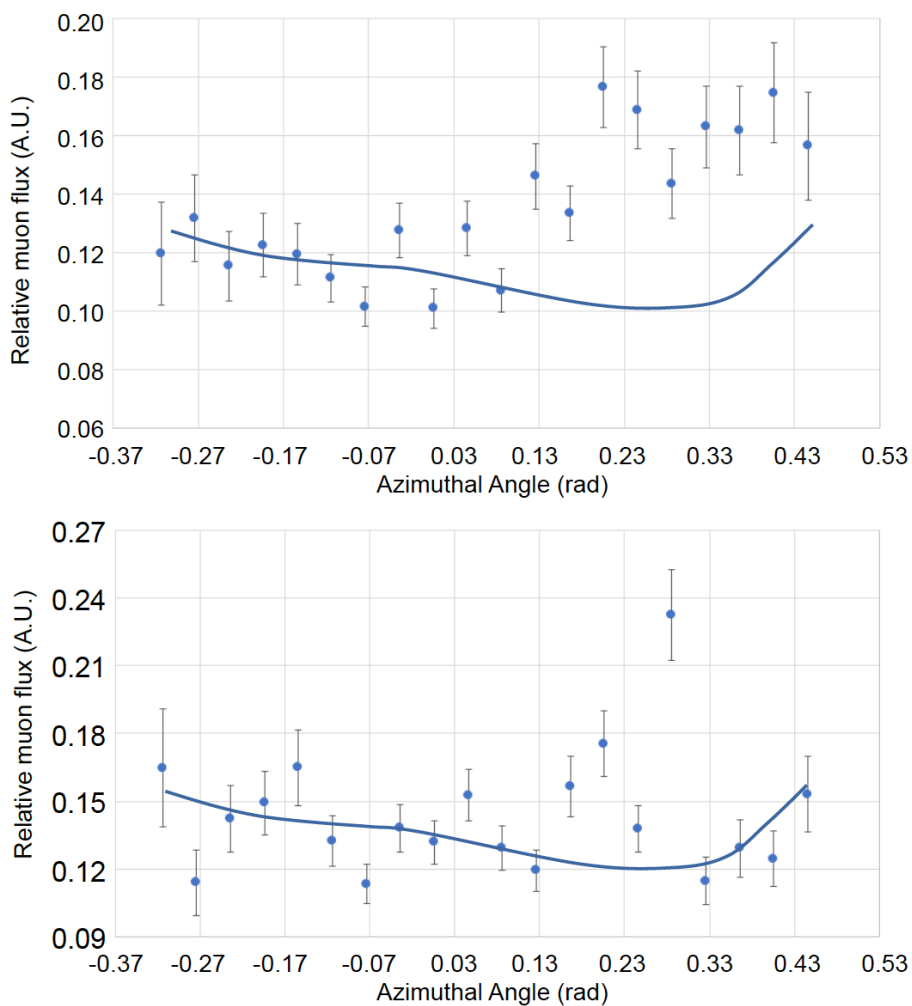
272
273 Figure 3. Angular distribution of the relative muon flux, as was observed from the
274 measurement at Position A. The horizontal and vertical bin widths are respectively 40
275 mrad and 8 mrad. The azimuthal distribution of the relative muon flux was normalized
276 to the total number of muons counted at each elevation angle.

277
278

279 Figure 4 shows the azimuthal distribution of the relative muon flux at shallow depths (at
280 elevation angles of 108 mrad (Figure 4A) and 100 mrad (Figure 4B)). The solid lines
281 are the expected muon flux. These lines were drawn based on the geometrical thickness
282 of the mound along the muon paths (Figure 1) by assuming the uniform density
283 distribution inside the mound. In these three images, the following three features can be
284 found. (A) Overall, the excessive flux of muons was observed in the positive azimuthal
285 angle region. This indicates that the average density in the positive azimuthal angle



286 region is lower than that in the negative angle region. An overall density variation
287 between them is 10-20%. (B) A strongly excessive muon flux can be found in the
288 azimuthal angle region between 176 mrad and 296 mrad in Figures 4A and 4B. The
289 statistical significance was more than 4σ . (C) In Figures 4A, there is also a low-density
290 region within the azimuthal angle range between 296-456 mrad. The position of this
291 low-density region corresponds to that of Trench F (dotted lines in Figure 1). From (A)
292 and (B), it was inferred that a large almost vertical crack exists in the shallow region,
293 however its existence was not clear when it's deeper than 2 m because of the effect of
294 overlapping the rectangular-shaped background mound (see the green-colored area at
295 the right bottom region of Figure 3). The density variations of this possible crack were
296 20-30% in comparison to the average density of the other part of the mound. The crack
297 width was 80-120 mrad that was equivalent to 6-8 m when considering the distance
298 between the detector and Crack A of 70 m.
299



300

301 Figure 4. Azimuthal distribution of the relative muon flux for elevation angles of 108
302 mrad (A), 100 mrad (B) and 92 mrad (C). The solid curves indicate the expected
303 horizontal muon flux variations.

304

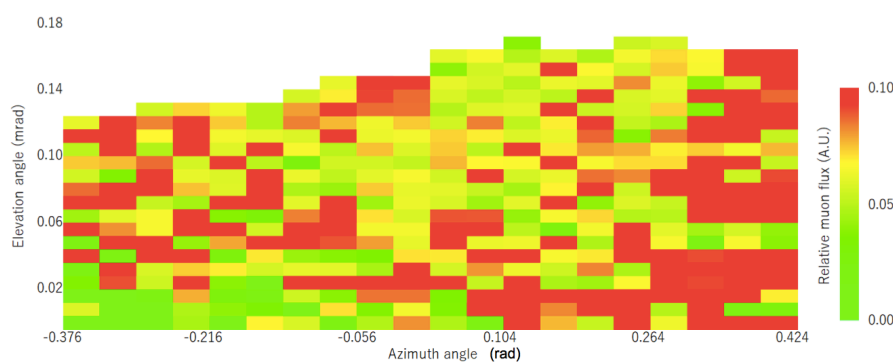
305

306 Crack A was not parallel to the muon's ray path at Position B (Figure 1), however,
307 Crack B was parallel to those in the azimuthal angle range between 300-420 mrad.

308 Therefore, it was expected that the similar structure to Crack A would be observed in
309 this angular region. Figure 5 shows the muographic image (Image B) taken at



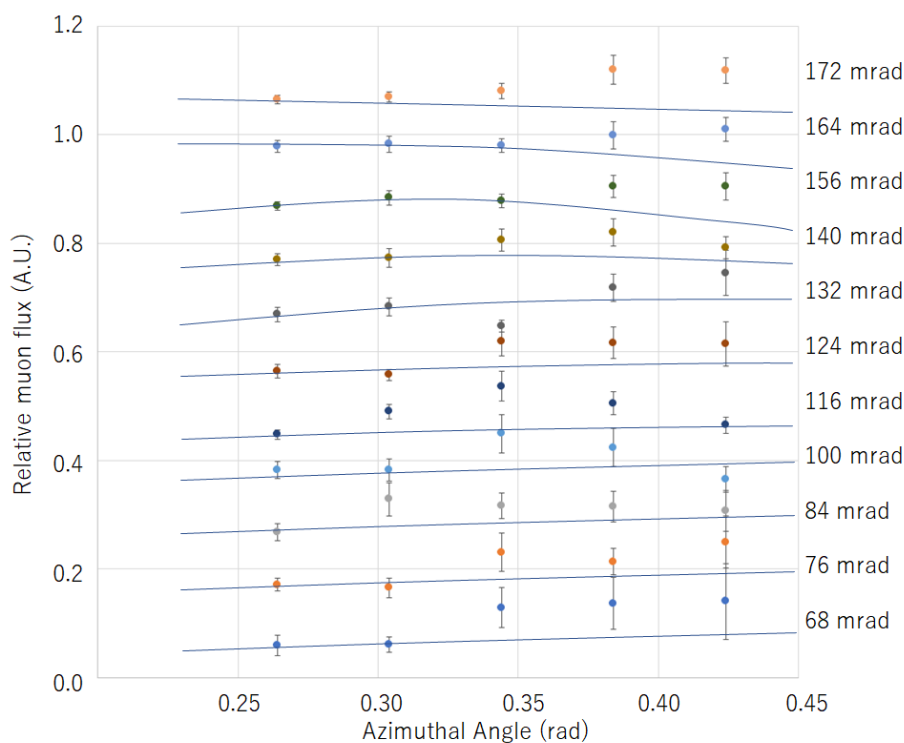
310 Position B. Since the distance to the mound peak (50 m) was closer at Position B,
311 almost doubly defined density structure was imaged. The data were normalized to the
312 azimuthal distribution of the muon tracks recorded within the elevational range between
313 300 and 360 mrad in order to derive the “relative muon flux”. Corresponding azimuthal
314 angles (-0.376 rad - 0.424 rad) are shown in Figure 1.
315



316
317 Figure 5. Angular distribution of the relative muon flux observed at Position B. The
318 horizontal and vertical bin widths are respectively 40 mrad and 8 mrad. The azimuthal
319 distribution of the relative muon flux was normalized to the total number of muons
320 counted at each elevation angle.

321
322
323 In Figure 6, the azimuthal distribution of the relative muon flux for elevation angles of
324 68 mrad - 172 mrad are shown. In these images, the excessive muon flux was found
325 within the azimuthal angle range between 264-424 mrad. The statistical significance
326 was overall more than 1σ . This low-density region was interpreted as the crack
327 associated with the same scalp (Scalp A), and it was found that the vertical extent of the
328 crack was much deeper than what could be seen in Image A. The crack width was at
329 least 80-160 mrad that was equivalent to 4-8 m when considering the distance between
330 the detector and Crack B. The reddish region in Figure 5 that can be seen on the left side
331 of Crack B indicates low-density collapsed landslide mass, with a mixture of the
332 remnant of the past excavation at Trench F.

333
334



335

336 Figure 6 Azimuthal distribution of the relative muon flux for various elevation angles.
337 The solid curves indicate the expected horizontal muon flux variations.

338

339

340 5. Discussion

341 From the bidirectional muographic images taken in the current measurements, the
342 following interpretations were derived.

343

344 (A) The reddish patches that can be seen on the left side of Images A and B indicate an
345 existence of a large-scaled collapsed landslide mass on the northern slope of the mound.
346 The collapsed landslide mass has a significant amount of the interparticle space; hence a
347 lower density in comparison to the surrounding regions.

348

349 (B) The vertical low-density regions at the top of the mound in Images A and B show
350 that there is a large-scale vertical crack behind Scalp A. The widths of these vertical
351 cracks were both 4-8 m thus it is reasonable to assume they are associated with the same



352 scalp.

353

354 In conclusion, the following picture was proposed. In prior trench-survey-based works,
355 most of the landslides that deformed this burial mound structure were found to have
356 been caused by a translational process. On the other hand, there was an exceptionally
357 large-scale rotational slide was found in the north region of the round-shaped section of
358 the mound, and the stone chamber was deformed and destroyed by this collapse process.
359 However, in the current muographic observations, a large-scale vertical crack was
360 discovered at the top of the round-shaped section, and it was found that the burial
361 mound deformation that connected to the translational collapse process also occurred
362 behind this rotational landslide. These data indicate that there was an intrinsic problem
363 with the stability of the basic foundation of the Imashirozuka mound before the 1596
364 Fushimi Earthquake. Changes in the foundation as a response to shaking from the
365 earthquake may have produced this large-scale burial mound collapse.

366

367 The burial mound seems to have a robust structure, more stable against earthquakes
368 than slender buildings like clock towers. However, a number of the ancient burial
369 mounds throughout Japan have collapsed from earthquakes and many modern buildings
370 are now built upon them. A small fraction has survived since early times, however, they
371 do not always indicate the earthquake-free sites. They represent an example of the final
372 designs of ancient Japanese construction since they have remained even after having
373 experienced a number of destructive earthquakes.

374

375 The technique of muography, which can probe seismically damaged ancient mounds is
376 similar to medical radiography which seeks to find the position, formation, and size of
377 the fractured zone inside the human body. In general, it is difficult to understand the
378 extent of damage, for example, of a patient's external wound without also understand
379 what is happening inside the body. The outside structure of ancient mounds is similar.
380 The surface of them has usually been naturally or artificially eroded with added
381 vegetation covering the shape during a long period of time it has existed. However, the
382 inside is more intact. For this reason, the trench survey technique (physically digging a
383 trench into the structure) to understand the "inside" can reveal valuable data.
384 However, similar to the manner in which x-ray photographs are usually applied to a
385 diagnosis before surgery is considered, muography is a more convenient and
386 noninvasive technique to effectively understand the overall inside structure to assess the
387 effect of time and natural disasters on the structure as a whole.



388

389 The current proof of concept measurement has attempted to show whether the technique
390 of muography increases the possibilities of finding more physical evidence related to
391 past earthquakes by selecting the Imashirozuka mound as an example. Obviously, the
392 specific earthquake damage of each burial mound is unique and cannot be generalized.
393 Its response depends not only on its material properties of the mound including its
394 mechanical properties of its foundations (strength and rigidity), but also on the ground
395 motion during an earthquake. Surveying and mapping various mounds that are thought
396 to be affected by the earthquake will provide a valuable data for us to verify and sort out
397 the factors that caused the damage.

398

399 Not only Imashirozuka mound but also other various burial mounds including the
400 Mishima mound group and the Kobo mound group are concentrated along the Rokkou
401 active fault system and its next neighbor Arima-Takatsuki tectonic line. The current
402 muographic results suggest that a combination of muography and the techniques of
403 trench survey or other conventional geophysical techniques can contribute towards the
404 construction of a more comprehensive understanding of the seismic response and
405 deformation of each burial mound. The characteristics of muography would allow
406 researchers to conduct an investigation of several sites quickly and efficiently to grasp
407 the general trend of the ensemble of these sites. Incorporating the muography
408 visualization technique into engineering expertise and in conjunction with historical
409 comparanda would utilize a new potential: by acquiring this new, valuable data from
410 these ancient burial mounds in Japan and other similar sites worldwide, we would
411 increase our ability to tackle future challenges of natural disaster preparation.

412

413 **Acknowledgements**

414 The authors acknowledge Toshitaka Kamai for valuable discussions about the current
415 muographic observation results. The authors also acknowledge Takefumi Hayashi for
416 his coordination and support the current measurements, Fumitaka Yoneda & Chikara
417 Inoue for their valuable archaeological advice, Ichiro Kanegae for provision of past
418 excavation research materials of Imashirozuka mound, and Masao Uchida for his
419 support as a chief administrator of Imashirozuka park.

420

421 **References**

422 Alvarez, L. W., Anderson, J. A., El Bedwei, F., Burkhard, J., Fakhry, A., Girgis, A.,
423 Goneid, A., Hassan, F., Iverson, D., Lynch, G., Miligy, Z., Moussa, A. H., Sharkawi, A.,



- 424 and Yazolino, L.: Search for hidden chambers in the pyramid, *Science*, 167, 832– 739,
425 doi:10.1126/science.167.3919.832, 1970.
426
- 427 Ambraseys NN., Banda E., Irving J., Mallard D., Melville C., Morse T., Muir-Wood R.,
428 Munoz D., Serva L., Shilston D., Surinach E., Vogt J.: Notes on Historical Seismicity.
429 *Bull. Seismol. Soc. Am.* 73(6), 1917–1920, 1983.
430
- 431 Carbone, D., Gibert, D., Marteau, J., Diament, M., Zuccarello, L., and Galichet, E.: An
432 experiment of muon radiography at Mt. Etna (Italy), *Geophys. J. Int.*, 196, 633–643,
433 2013.
434
- 435 Cimmino, L., Baccani, G., Noli, P., Amato L., Ambrosino, F., Bonechi, L., Bongi, M.,
436 Ciulli, V., D’Alessandro, R., D’Errico, M., Gonzi, S., Melon, B., Minin, G., Saracino,
437 G., Scognamiglio, L., Strolin P., Viliani, L.: 3D Muography for the Search of Hidden
438 Cavities, *Scientific Reports* 9, 2974, 2019.
439
- 440 Daly, P., Sieh, K., Yew Seng, T., McKinnon, EE., Parnell, AC., Ardiansyah, R., Feener,
441 M., Ismail, N., Nizamuddin, Majewski J.: Archaeological evidence that a late
442 14th-century tsunami devastated the coast of northern Sumatra and redirected history,
443 *PNAS*, 116 (24) 11679-11686, 2019
444
- 445 Dey, H., Goodman-Tchernov, B., Sharvit, J.: Archaeological evidence for the tsunami
446 of January 18, A.D. 749: a chapter in the history of Early Islamic Qaysariyah (Caesarea
447 Maritima), *Journal of Roman Archaeology*, 27, 357-373, 2014.
448
- 449 Elson, M., Ort, M.H.: *Archaeological Volcanology*, The Encyclopedia of
450 Archaeological Sciences. Edited by Sandra L. López Varela. John Wiley & Sons, Inc.,
451 1-5, 2018.
452
- 453 Guardincerri E., Bacon JD., Barros N., Blasi C., Bonechi L., Chen A., D’Alessandro R.,
454 Durham JM., Fine M., Mauger C., Mayers G., Morris C., Newcomer FM., Okasinski J.,
455 Pizzico T., Plaud-Ramos K., Poulson DC., Reilly MB., Roberts A., Saeid T., Vaccaro
456 V., Van Berg R.: Imaging the dome of Santa Maria del Fiore using cosmic rays, *Philos.*
457 *Trans. A Math. Phys. Eng. Sci.* 377 (2137) 20180136, 2018. doi:
458 10.1098/rsta.2018.0136.
459



- 460 Guidoboni, E., Comastri, A., Traina G., Catalogue of Ancient Earthquakes in the
461 Mediterranean Area up to the 10th Century, Istituto Nazionale di Geofisica, Rome,
462 1994.
- 463
- 464 Hanazato, T., Tanaka, HKM.: Inspection of the internal structure of the
465 UNESCO-World Heritage with cosmic rays, *Isotope News*, 741, 60-64, 2016.
- 466
- 467 Kamai, T., Sangawa, A., Shuzui, H.: Landslides on Ancient Burial Mounds Induced by
468 the 1596 Keicho-Fushimi Earthquake, *Jour. Japan Soc, Eng. Geol.*, 48, 6, 285-298,
469 2008.
- 470
- 471 Korjenkov, AM., Mazor E.: Archaeoseismology in Mamshit, Southern Israel, cracking a
472 millennia-old code of earthquake preserved in ancient ruins, *Archäologischer Anzeiger*,
473 2, 51-82, 2003.
- 474
- 475 Lesparre, N., Gibert, D., Marteau, J., Komorowski, J.-C., Nicollin, F., and Coutant, O.:
476 Density muon radiography of La Soufriere of Guadeloupe volcano: comparison with
477 geological, electrical resistivity and gravity data, *Geophys. J. Int.*, 190, 1008–1019,
478 2012.
- 479
- 480 Mahon D., Clarkson A., Gardner S., Ireland D., Jebali R., Kaiser R., Ryan M., Shearer
481 C., Yang G.: First-of-a-kind muography for nuclear waste characterization, *Philos.*
482 *Trans. A Math. Phys. Eng. Sci.* 377 (2137) 20180048, 2018. doi:
483 10.1098/rsta.2018.0048.
- 484
- 485 Morishima K., Kuno M., Nishio A., Kitagawa N., Manabe Y., Moto M., Takasaki F.,
486 Fujii H., Satoh K., Kodama H., Hayashi K., Odaka S., Procureur S., Attié D., Bouteille
487 S., Calvet D., Filosa C., Magnier P., Mandjavidze I., Riallot M., Marini B., Gable P.,
488 Date Y., Sugiura M., Elshayeb Y., Elnady T., Ezzy M., Guerriero E., Steiger V.,
489 Serikoff N., Mouret JB., Charlès B., Helal H., Tayoubi M.: Discovery of a big void in
490 Khufu's Pyramid by observation of cosmic-ray muons, *Nature*, 552(7685), 386-390,
491 2017. doi: 10.1038/nature24647
- 492
- 493 Olah L., Tanaka, HKM., Ohminato T., Hamar G., Varga D.: Plug Formation Imaged
494 Beneath the Active Craters of Sakurajima Volcano With Muography, *Geophys. Res.*
495 *Let.*, GL084784, 2019. doi.org/10.1029/2019GL084784.



- 496
497 Olah, L., Barnaföldi, G. G., Hamar, G., Melegh, H. G., Surányi, G., and Varga, D.:
498 CCC-based muon telescope for examination of natural caves, *Geosci. Instrum. Method.*
499 *Data Syst.*, 1, 229–234, doi:10.5194/gi-1-229-2012, 2012.
- 500
501 Olah L., Tanaka HKM., Ohminato T., Varga D.: High-definition and low-noise
502 muography of the Sakurajima volcano with gaseous tracking detectors, *Sci Rep.* 8(1),
503 3207, doi: 10.1038/s41598-018-21423-9, 2018.
- 504
505 Sangawa, A., Miyazaki, Y.: Traces of Landslides found in Imashirosuka mound, 18th
506 meeting of Japan Society for Scientific Studies on Cultural Property, 24-25, 2001.
- 507
508 Schouten, D.: Muon geotomography: selected case studies, *Philos. Trans. A Math. Phys.*
509 *Eng. Sci.* 377 (2137) 20180061, doi: 10.1098/rsta.2018.0061, 2018.
- 510
511 Tanaka, H. K. M., Nakano, T., Takahashi, S., Yoshida, J., Takeo, M., Oikawa, J.,
512 Ohminato, T., Aoki, Y., Koyama, E., Tsuji, H., and Niwa, K.: High resolution imaging
513 in the inhomogeneous crust with cosmic-ray muon radiography: The density structure
514 below the volcanic crater floor of Mt. Asama, Japan, *Earth Planet. Sc. Lett.*, 263, 104–
515 113, 2007.
- 516
517 Tanaka, H. K. M., Uchida, T., Tanaka, M., Takeo M., Oikawa J., Ohminato T., Aoki Y.,
518 Koyama, E., Tsuji H.: Detecting a mass change inside a volcano by cosmic-ray muon
519 radiography (muography): First results from measurements at Asama volcano, Japan,
520 *Geophys. Res. Lett.*, GL039448, doi.org/10.1029/2009GL039448, 2009.
- 521
522 Tanaka, H. K. M., Miyajima, H., Kusagaya, T., Taketa, A., Uchida, T., and Tanaka, M.:
523 Cosmic muon imaging of hidden seismic fault zones: Raineater permeation into the
524 mechanical fracture zone in Itoigawa-Shizuoka Tectonic Line, Japan, *Earth Planet. Sc.*
525 *Lett.*, 306, 156–162, 2011.
- 526
527 Tanaka H.K.M., Kusagaya T., Shinohara H., Radiographic visualization of magma
528 dynamics in an erupting volcano, *Nat Commun.* 10, 5, 3381, doi: 10.1038/ncomms4381,
529 2014.
- 530
531 Tanaka, H. K. M.: Development of stroboscopic muography, *Geosci. Instrum. Method.*



532 Data Syst., 2, 41–45, doi:10.5194/gi-2-41-2013, 2013.
533
534 Tanaka, H. K. M., Ohshiro, M.: Muographic data analysis method for medium-sized
535 rock overburden inspections, Geosci. Instrum. Method. Data Syst., 5, 427–435,
536 doi:10.5194/gi-5-427-2016, 2016.
537
538 Tanaka H. K. M., Muraoka, H.: Interpreting muon radiographic data in a fault zone:
539 possible application to geothermal reservoir detection and monitoring, Geosci. Instrum.
540 Method. Data Syst., 2, 145–150, <https://doi.org/10.5194/gi-2-145-2013>, 2013
541
542
543
544